Bull. Mater. Sci., Vol. 40, No. 2, April 2017, pp. 367–373. © Indian Academy of Sciences.
DOI 10.1007/s12034-017-1380-6

Effect of magnetite nanoparticles on dye absorption properties of magnetite@carbon composites

YUNFANG LIU[1,*], YANGYANG LI[1], XIN ZHAO[1], WEIDONG CHI[1], QIGU HUANG[1], CHANGYUAN YU[2] and YONG XIANG[3]

[1]Key Laboratory of Carbon Fibers and Functional Polymers of Ministry of Education, Beijing University of Chemical Technology, Beijing 100029, People's Republic of China
[2]College of Life Science and Technology, Beijing University of Chemical Technology, Beijing 100029, People's Republic of China
[3]Sinopuri Environment Engineering Science and Technology (Shanghai) Co. Ltd, Shanghai 200090, People's Republic of China

MS received 8 December 2015; accepted 7 July 2016

Abstract. **Magnetite@carbon (Fe_3O_4@C) composites were prepared using three kinds of Fe_3O_4 nanoparticles (NPs). All the Fe_3O_4@C composites could be easily separated from water by an external magnet. The Fe_3O_4 NPs synthesized by a microreactor system have the smallest size and narrowest size distribution among the three kinds of Fe_3O_4 NPs. The saturated capacity of the Fe_3O_4@C composite originating from microreactor-prepared Fe_3O_4 NPs to absorb Rhodamine B at 20°C exceeds 135 mg g^{-1}, which is 1.35 times as much as the value of the Fe_3O_4@C composite originating from traditional Fe_3O_4 NPs. This value for the Fe_3O_4@C composite using commercial Fe_3O_4 NPs as core is only 76 mg g^{-1}. The Fe_3O_4@C composite using microreactor-prepared Fe_3O_4 NPs also has good retrievability and reusability.**

Keywords. **Magnetite; carbon composite; microreactor; absorption property.**

1. Introduction

Treatment technologies for dye-containing wastewater have become more and more important, especially for paper making, plastics, printing and textiles, due to its bad biodegradability. Adsorption is an effective and attractive process. Many adsorbents have been used, such as metal oxides and carbon materials [1–4]. Recently, magnetite@carbon (Fe_3O_4@C) composites have also attracted great attention as adsorbents due to their excellent absorption ability and high separation efficiency. Many methods were used for Fe_3O_4@C composites with different Fe_3O_4 cores [5–11]. Fe_3O_4 cores are one of the key factors for excellent property of Fe_3O_4@C composite, whose structure and property have great impact on the properties of Fe_3O_4@C composites. Many methods have been developed for preparation of Fe_3O_4 nanoparticles (NPs), such as hydrothermal or solvothermal method, sol–gel method, coprecipitation method, reflux method and ball milling method [12–18]. Compared with other methods, the coprecipitation method (traditional adding method) has some advantages due to its simplicity, high applicability and high product purity [18]. But Fe_3O_4 NPs prepared by this method still suffer some shortcomings, such as relatively large particle size, wide size distribution and severe aggregation [18]. These problems will obviously impair the properties of Fe_3O_4@C composites. Microreactors as a small reaction system could provide efficient repeatability and highly selective production of NPs due to their unique geometric features (microscale, large specific surface area, small volume and unique fluid behaviour) [19–22]. Therefore, NPs with certain size and uniform size distribution could be obtained more easily. In this work, we synthesized Fe_3O_4 NPs using a microreactor system for Fe_3O_4@C composite. For comparison, Fe_3O_4 NPs from the traditional adding method and commercial samples were also used. The structure and magnetic and dye absorption properties of Fe_3O_4@C composites were investigated.

2. Experimental

2.1 *Materials*

Ferrous sulphate ($FeSO_4 \cdot 7H_2O$), ferric trichloride ($FeCl_3 \cdot 6H_2O$) and commercial Fe_3O_4 NPs were bought from Beijing Modern Oriental Fine Chemicals Co., Ltd. Soluble starch ($(C_6H_{10}O_5)_n$) and NaOH were obtained from Beijing Yili Fine Chemicals Co., Ltd. Rhodamine B (RhB) was purchased from Tianjin Guangfu Fine Chemical Research Institute. In our study, all chemicals used were of analytical grade.

2.2 *Synthesis of Fe_3O_4 NPs and Fe_3O_4@C composites*

Fe_3O_4 NPs were prepared by two methods (microfluid synthesis and traditional coprecipitation synthesis). For the

*Author for correspondence (liuyunfang@mail.buct.edu.cn)

former, 120 ml of aqueous solution A (1.151 g of $FeCl_3 \cdot 6H_2O$ and 0.778 g of $FeSO_4 \cdot 7H_2O$) and 120 ml of aqueous solution B (0.9 g of NaOH) were synchronously pumped at a constant flow rate (20 ml min^{-1}) into two inlets of a micromixer connected with a PTFE capillary tube (ID: 0.5 mm, length: 1 m) at the outlet (labelled as MR-Fe_3O_4). For the latter, 120 ml of solution A was dropped into solution B (120 ml) with mechanical agitation and ultrasound (labelled as TA-Fe_3O_4). The commercial Fe_3O_4 sample was labelled as C-Fe_3O_4.

To prepare Fe_3O_4@C composites, Fe_3O_4 NPs (0.65 g), soluble starch (3 g) and H_2O (55 ml) were mixed and transferred to a Teflon-sealed autoclave and kept at 180°C for 20 h. The solid product was magnetically separated, and repeatedly rinsed with water and ethanol several times. After that, the Fe_3O_4@C composites were dried overnight at 65°C (correspondingly labelled as MR-Fe_3O_4@C, TA-Fe_3O_4@C and C-Fe_3O_4@C).

2.3 *Adsorption characterization*

RhB was used as a model compound to evaluate the adsorption property of the Fe_3O_4@C composites. Each batch experiment was performed as follows: firstly, RhB solution (1 g l^{-1}, 100 ml) was prepared and its pH value was adjusted to be in the range of 3–11 using HCl or NaOH solutions; secondly, the absorbing material (0.1 g) was added into this solution with agitation for a certain time; then, the magnetic materials were separated from the solution using a magnet, and the RhB concentration was measured using a UV–vis spectrophotometer at the wavelength of 554 nm. The adsorption capacity at different times (q_t) was calculated using the following equation:

$$q_t = (C_0 - C_t)/C_a \quad (1)$$

In this equation, C_0 is the initial concentration of RhB, C_t is the concentration of RhB at different absorption times and C_a is the concentration of absorption material.

To evaluate the reusability of Fe_3O_4@C composite, regeneration experiment was performed as follows: (1) after saturated adsorption, Fe_3O_4@C composite was separated from water and simply washed with deionized water several times; (2) after drying, the recovered Fe_3O_4@C composite was used for the next adsorption experiment.

2.4 *Recovery experiment*

The recovery experiment was performed as follows: (1) Fe_3O_4@carbon composite (50 mg) was added into deionized water (100 ml) and dispersed by agitation; (2) Fe_3O_4@carbon composite was separated from water by an external magnet and kept in an oven to dry at 110°C for 12 h; (3) The dried sample was weighed and the recovery η was calculated according to the following equation:

$$\eta = (m/m_0) \times 100\%. \quad (2)$$

In this equation, m_0 is the initial mass of Fe_3O_4@carbon composite and m is the mass of the recovered Fe_3O_4@carbon composite.

2.5 *Structural characterization*

The microstructures and crystal structures of the samples were characterized by transmission electron microscopy (TEM, FEI, Tecnai-G2) and X-ray diffraction (XRD, Rigaku, D/Max2500 VB2+/PC, CuKα, Kα = 0.15418 nm, 40 kV, 200 mA), respectively. The surface and magnetic properties of the samples were analysed using an infrared spectrum analyzer (IR, TNZ1-5700) and a vibrating sample magnetometer (EG & GVSM Model 155), respectively. The surface states of the materials were characterized by X-ray photoelectron spectra (XPS, Thermo Fisher Scientific, Escalab250).

3. Results and discussion

The TEM images of Fe_3O_4 samples and their statistical size-distribution histograms are showed in figure 1. It can be observed that C-Fe_3O_4 NPs and TA-Fe_3O_4 NPs suffer more serious aggregation than MR-Fe_3O_4 NPs. The average particle sizes of C-Fe_3O_4, TA-Fe_3O_4 and MR-Fe_3O_4 are about 28.2, 11.7 and 9.7 nm, respectively. MR-Fe_3O_4 NPs have the smallest size and narrowest size distribution among them. The nucleation and growth of MR-Fe_3O_4 NPs could be divided and controlled well because of the tiny channel and strong mass transmittability of the microreactor [19,20]. As a result, Fe_3O_4 NPs with narrow size distribution and good dispersion were obtained. The TEM images of Fe_3O_4@C composites (figure 2) clearly show the carbon encapsulation of Fe_3O_4 NPs.

Figure 3 shows the XRD patterns of Fe_3O_4 and Fe_3O_4@C composites. All Fe_3O_4 samples have the standard diffraction peaks of Fe_3O_4 material with a cubic spinel structure of Fe_3O_4 (JCPDS No. 19-0629). In these patterns, the distinct peaks at 30.2, 35.6, 43.2, 53.7, 57.2 and 62.8° of 2θ are assigned to crystal planes (220), (311), (400), (422), (511) and (440), respectively. The lattice spacing value of about 0.253 nm for (311) crystal plane is in accordance with the JCPDS database (JCPDS No. 19-0629). According to the Scherrer equation using (311) diffraction peak, the sizes of C-Fe_3O_4, TA-Fe_3O_4 and MR-Fe_3O_4 are about 27.3, 13.8 and 9.8 nm, respectively. These results agree with the TEM data. In the patterns of C-Fe_3O_4 and C-Fe_3O_4@C, a small peak appearing at about 37.1° of 2θ is attributed to crystal plane (222). Actually, the other patterns also have this peak. But the peak intensity is very weak. It is possible that C-Fe_3O_4 has relatively big size and high crystallinity. No obvious new diffraction peak appears in the XRD pattern of Fe_3O_4@C composites, demonstrating the amorphous structure of the carbon shell. The FTIR spectra of Fe_3O_4 and Fe_3O_4@C composites are shown in figure 4. The wide strong peak in the range of 55–580 cm^{-1} is contributed to Fe–O stretching vibration of Fe_3O_4 [23–26]. It is well known that

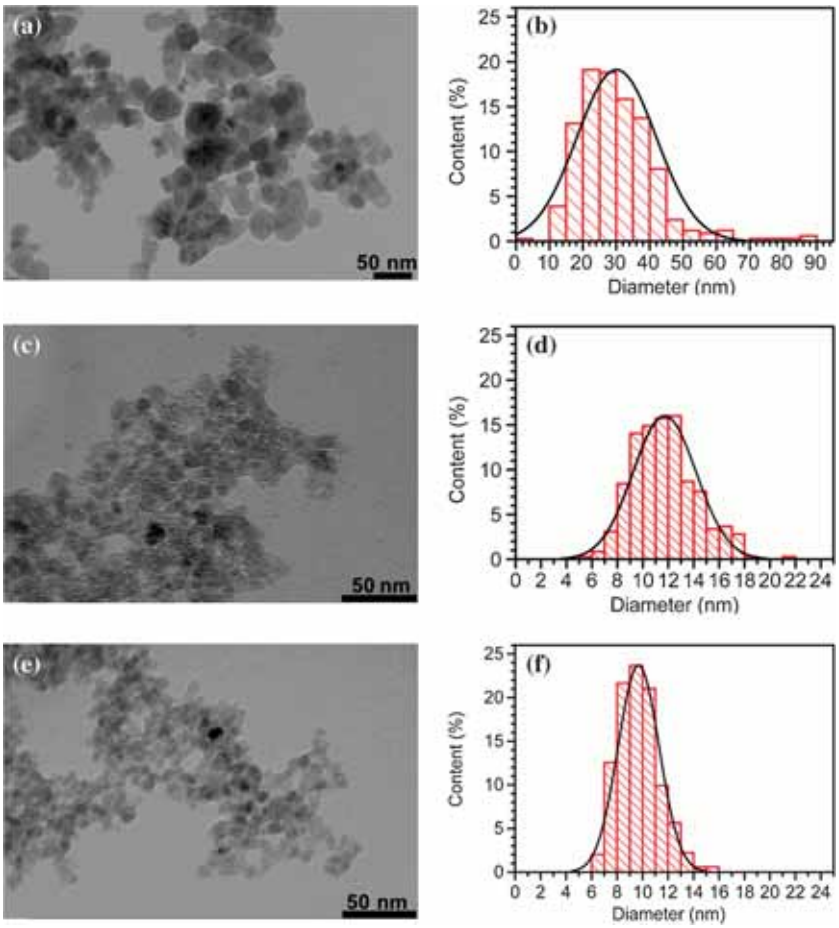

Figure 1. TEM images and statistical size-distribution histograms, respectively, of (**a**, **b**) C-Fe_3O_4, (**c**, **d**) TA-Fe_3O_4 and (**e**, **f**) MR-Fe_3O_4.

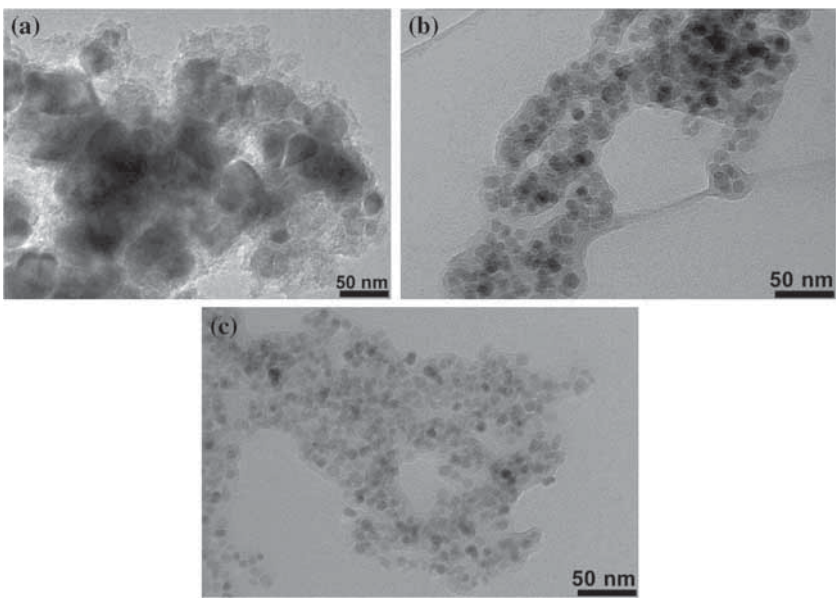

Figure 2. TEM images of (**a**) C-Fe_3O_4@C, (**b**) TA-Fe_3O_4@C and (**c**) MR-Fe_3O_4@C.

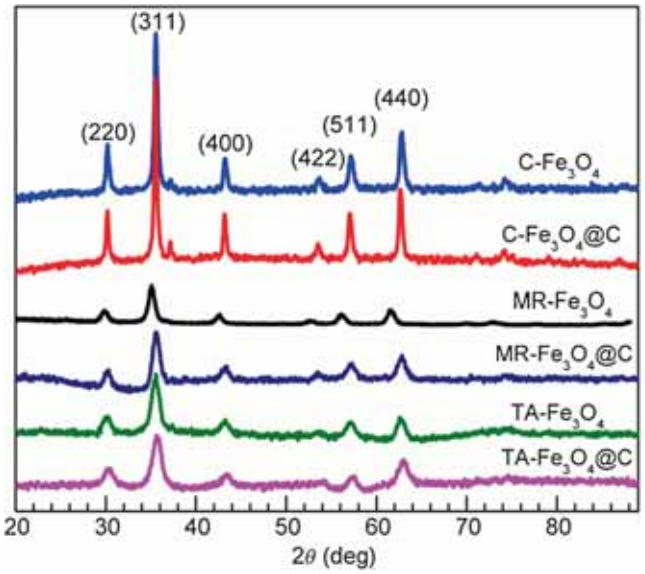

Figure 3. XRD patterns of Fe_3O_4 and Fe_3O_4@C composites.

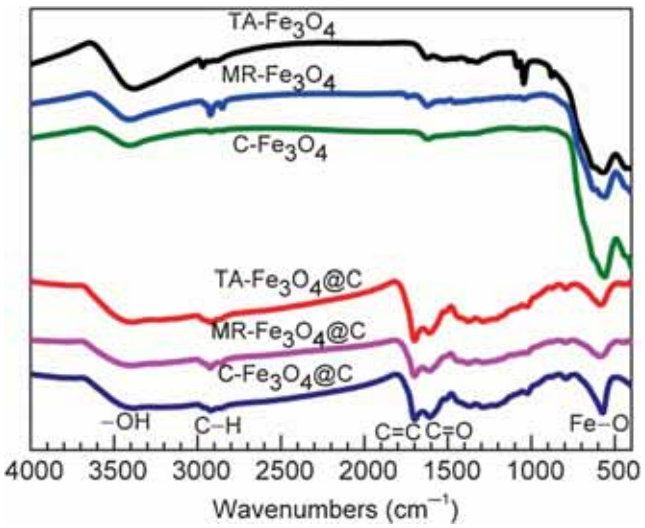

Figure 4. FTIR spectra of Fe_3O_4 NPs and Fe_3O_4@C composites.

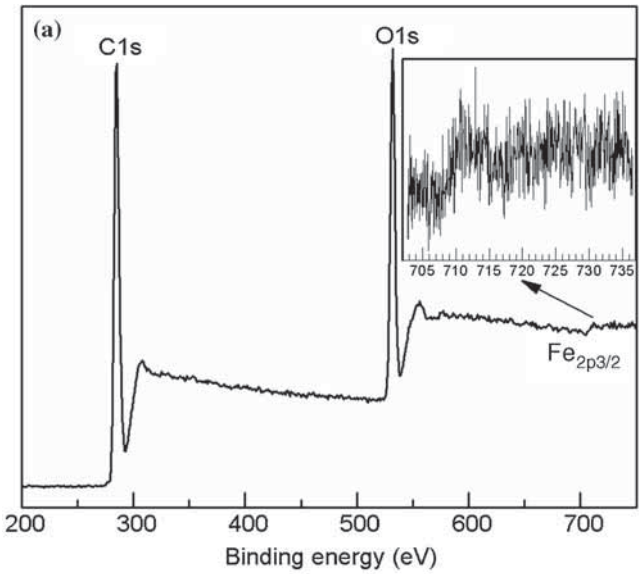

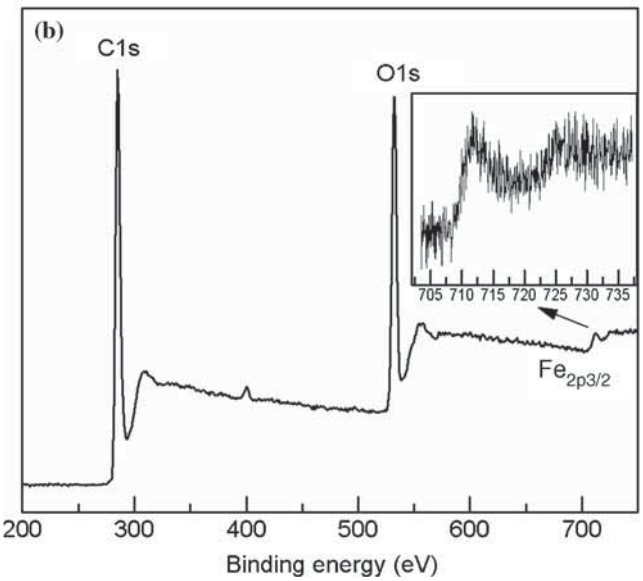

Figure 5. XPS spectra of (**a**) TA-Fe_3O_4@C and (**b**) MR-Fe_3O_4@C.

the absorption band of nanomaterial becomes wide with the decrease of its size. This is possibly the main reason for the wide peak shape. The shape difference of Fe–O stretching vibration peak between Fe_3O_4 and Fe_3O_4@C may originate from the carbon encapsulation of Fe_3O_4. The peaks at 1600 and 1696 cm^{-1} are characteristics of C=O and C=C vibrations [27]. The weak peak at 3377 cm^{-1} belongs to vibration of –OH group [28]. The broad region from 2780 to 3000 cm^{-1} is assigned to C–H vibration. The existence of C–H, C=O and C=C clearly demonstrates the existence of carbon. Figure 5 displays the XPS spectra of Fe_3O_4@C composites. The two main peaks for Fe_3O_4@C composites are located at about 285 and 532.7 eV which correspond to C1s and O1s peaks, respectively. The carbon contents of both Fe_3O_4@C composites are beyond 70%. The enlarged Fe2p peaks ($Fe_{2p1/2}$ and $Fe_{2p3/2}$) for both composites were interpolated in figure 5. The results demonstrate that Fe_3O_4 NPs have been encapsulated by a carbon layer. Figure 6a presents the magnetization hysteresis loops of Fe_3O_4 and Fe_3O_4@C composites at room temperature. All of the samples possess superparamagnetic property. The remnant magnetization values of C-Fe_3O_4, TA-Fe_3O_4 and MR-Fe_3O_4 are only 0.55, 0.13 and 0.12 emu g^{-1}, respectively. The saturation magnetization values (M_s) of C-Fe_3O_4, MR-Fe_3O_4 and TA-Fe_3O_4 are 67.3, 64.0 and 56.1 emu g^{-1}, respectively. The corresponding values of C-Fe_3O_4@C, MR-Fe_3O_4@C and TA-Fe_3O_4@C composites are respectively 45.5, 19.0 and 16.5 emu g^{-1}. As we know, the ferromagnetic response of the superparamagnetic particle decreases with the reduction of its size. Of course, the ferromagnetic response is also related to its crystallinity.

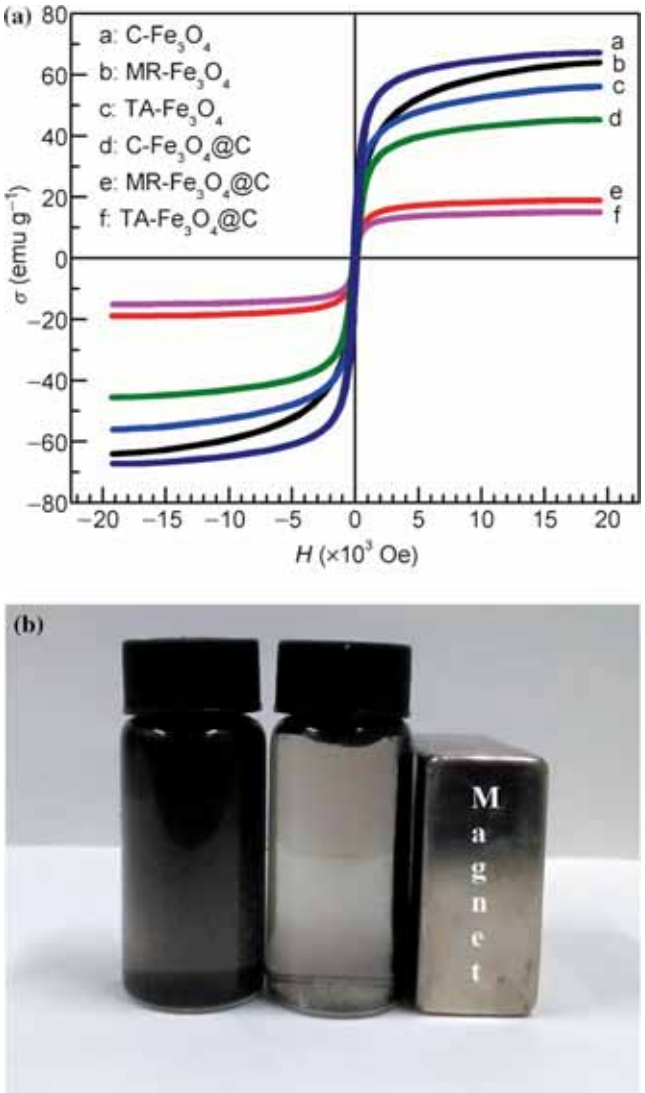

Figure 6. (**a**) Magnetic hysteresis loops of Fe_3O_4 and Fe_3O_4@C composites. (**b**) Photograph of an aqueous suspension of MR-Fe_3O_4@C and its separation by an external magnet.

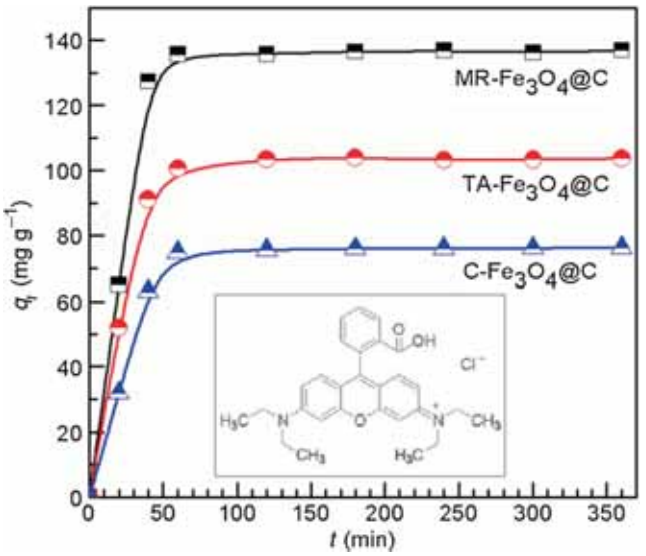

Figure 7. RhB isothermal absorption curves of Fe_3O_4@C composites.

The relatively large M_s values of C-Fe_3O_4 and C-Fe_3O_4@C composite are mainly attributed to the big size and high crystallinity of C-Fe_3O_4 NPs. That the MR-Fe_3O_4 NPs have relatively stronger M_s than that of the TA-Fe_3O_4 NPs may be related to crystallinity and defect of NPs [29,30]. It has been reported that 16.3 emu g^{-1} of M_s is enough for magnetic separation via alternative magnetic field [31]. Figure 6b shows a photograph of an aqueous suspension of MR-Fe_3O_4@C (left) and its separation by an external magnet (right). Its recovery η exceeds 99.1%. The magnetic properties of Fe_3O_4@C make them easily separated from water, which exhibits its potential as a magnetic adsorbent.

RhB was used as a model compound to evaluate the adsorption property of the Fe_3O_4@C composites. Firstly, the time required to achieve adsorption equilibrium was determined, which was carried at 20°C and pH value of 3. The absorption capacities of the Fe_3O_4@C composites rise rapidly and reach equilibrium values after about 60 min. RhB is a cationic dye (inset in figure 7). The electrostatic interaction between Fe_3O_4@C composites and RhB is one of the important factors affecting the adsorption ability [23,32]. Furthermore, adsorption ability will also be strengthened due to hydrogen bonds between hydroxyl groups and carbonyl groups [33,34]. The saturation capacity of MR-Fe_3O_4@C composite exceeds 135 mg g^{-1}, whereas the values of C-Fe_3O_4@C and TA-Fe_3O_4@C composites are only about 76 and 100 mg g^{-1}, respectively. Absorbing properties of only MR-Fe_3O_4@C and TA-Fe_3O_4@C were compared in the following discussion due to the relatively weak absorption capacity of C-Fe_3O_4@C composite. Figure 8a shows the effect of temperature on the saturation absorption of the composites (pH of 3 and 60 min of contact time). It is evident that the adsorption capacities increase with the increase of absorption temperature and reach the maximum values at 60°C (149 and 177 mg g^{-1} for TA-Fe_3O_4@C and MR-Fe_3O_4@C, respectively). This may be attributed to the generation of some new active sites on the surface of absorption materials due to bond rupture [35]. In addition the higher collision probability between RhB and adsorbent could also enhance the adsorption capacity. The corresponding absorption capacities drop to 141 and 170 mg g^{-1} at 70°C. Figure 8b displays the effect of initial pH on RhB adsorption capacity at 20°C. When the pH value increases from 3 to 9, the adsorption capacities of TA-Fe_3O_4@C and MR-Fe_3O_4@C respectively increase from 104 and 135 mg g^{-1} to 122 and 155 mg g^{-1}. In the range of 9–11, the adsorption capacities for both adsorbents decreased slightly. At lower pH, the adsorption of H^+ on the surface of adsorbent makes it positively charged. The increase of pH value leads to the negatively charged sites. When the adsorbent surface becomes negatively charged, the adsorption capacity reaches the maximum due to the strong electrostatic attraction between

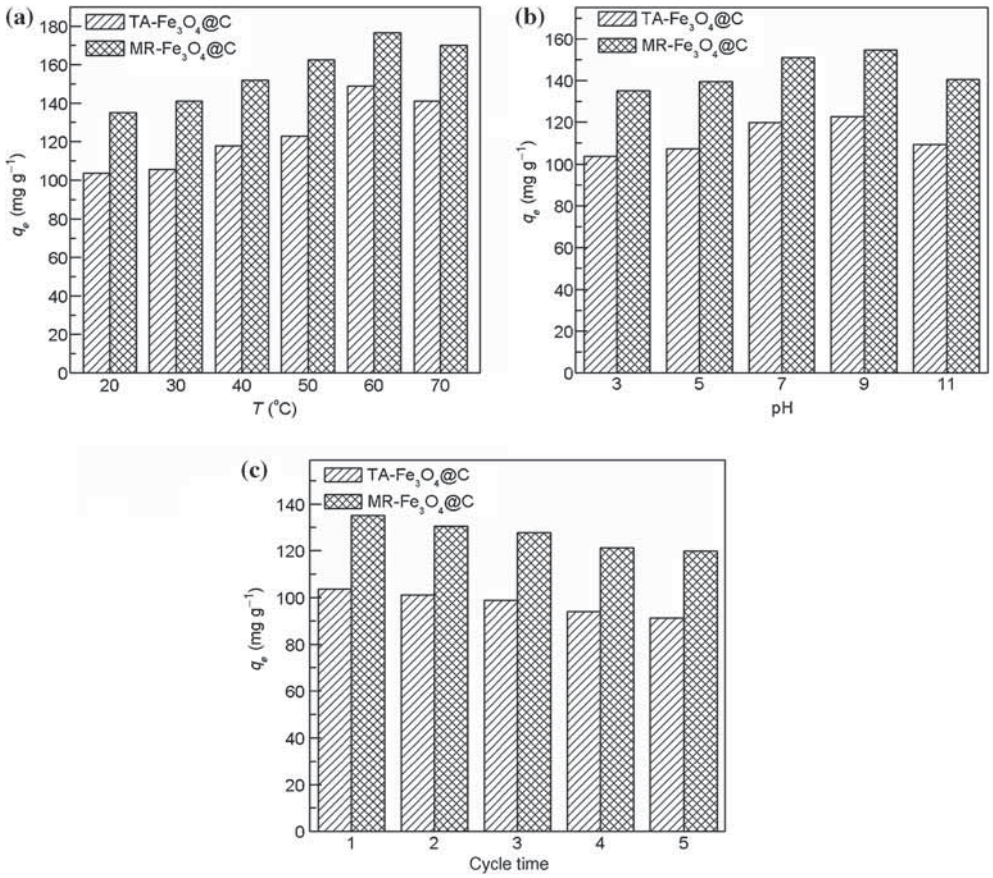

Figure 8. Effect of (**a**) temperature, (**b**) pH and (**c**) cycle time on absorption capacity of Fe_3O_4@C composites.

the adsorbent and RhB [36]. At much higher pH, the ion form of RhB changes from monomeric form to zwitterionic form, which leads to RhB aggregate [37]. The steric effect will hinder the absorption of RhB molecule on adsorbent. After adsorption, the adsorbents were simply regenerated by washing with deionized water. As seen in figure 8c, the adsorption capacities of TA-Fe_3O_4@C and MR-Fe_3O_4@C respectively decrease from 104 and 135 to 92 and 120 mg g^{-1} after four cycles. The Fe_3O_4@C composites still have excellent adsorption ability. The results indicate that both TA-Fe_3O_4@C and MR-Fe_3O_4@C could be reused, especially for MR-Fe_3O_4@C composite

4. Conclusions

Fe_3O_4@C composites were prepared by hydrothermal method using three kinds of Fe_3O_4 NPs as core: one from traditional coprecipitation, one from a microreactor and commercial Fe_3O_4. The Fe_3O_4 NPs from the microreactor have the smallest average size and size distribution among them. The Fe_3O_4@C composite using microreactor-prepared Fe_3O_4 NPs with 19.0 emu g^{-1} of saturated magnetization could be easily separated from water by a magnet. Its RhB saturation absorption capacity at relatively optimal condition exceeds 177 mg g^{-1} which is much larger than that of the other two composites. This Fe_3O_4@C composite also has excellent reusability.

Acknowledgements

This work was supported by the Fundamental Research Funds for the Central Universities of China (JD1406) and the National Natural Science Foundation of China (21174011, U1462102).

References

[1] Zhang F, Liu Y J, Xiao X C, Cai X Y, Li H and Wang Y D 2012 *Mater. Technol.* **27** 196
[2] Zhang F, Liu Y J, Liu Q H, Li Q, Li H, Cai X Y and Wang Y D 2013 *Mater. Technol.* **28** 310
[3] Mahmoodi N M and Masrouri O 2015 *J. Solution Chem.* **44** 1568
[4] Farahani Z H, Mahmoodi N M and Monfared H H 2015 *Fiber. Polym.* **16** 1035
[5] Zhang S X, Niu H Y, Hu Z J, Cai Y Q and Shi Y L 2010 *J. Chromatogr. A* **1217** 4757
[6] Zhang Y X, Xu S C, Luo Y Y, Pan S S, Ding H L and Li G H 2011 *J. Mater. Chem.* **21** 3664
[7] Fan W, Gao W, Zhang C, Tjiu W W, Pan J S and Liu T X 2012 *J. Mater. Chem.* **22** 25108

[8] Liang L, Zhu Q C, Wang T B, Wang F X, Ma J, Jing L Q and Sun J M 2014 *Micropor. Mesopor. Mater.* **197** 221

[9] Shi S, Fan Y W and Huang Y M 2013 *Ind. Eng. Chem. Res.* **52** 2604

[10] Zhang C, Mo Z L, Zhang P, Feng C and Guo R B 2013 *Mater. Lett.* **106** 107

[11] Zhao L Q, Chang X L, Liao R, Zhang X L, Xie J R, Yu B W, Wu R H, Wang R J and Yang S T 2014 *Mater. Lett.* **135** 154

[12] Cai W and Wan J Q 2007 *J. Colloid. Interf. Sci.* **305** 366

[13] Wang J, Chen Q W, Zeng C and Hou B Y 2004 *Adv. Mater.* **16** 137

[14] Tang N J, Zhong W, Jiang H Y, Wu X L, Liu W and Du Y W 2004 *J. Magn. Magn. Mater.* **282** 92

[15] Chen M J, Shen H, Li X and Liu H F 2014 *Appl. Surf. Sci.* **307** 306

[16] Meng H N, Zhang Z Z, Zhao F X, Qiu T and Yang J D 2013 *Appl. Surf. Sci.* **280** 679

[17] Karaoglu E, Baykal A, Deligoz H, Senel M, Sozeri H and Toprak M S 2011 *J. Alloys Compd.* **509** 8460

[18] Tao K, Dou H J and Sun K 2008 *Colloid. Surf. A* **320** 115

[19] Jahnisch K, Hessel V, Lowe H and Baerns M 2004 *Angew. Chem. Int. Ed. Engl.* **43** 406

[20] Song Y J, Hormes J and Kumar C S S R 2008 *Small* **4** 698

[21] Jensen K F 2001 *Chem. Eng. Sci.* **56** 293

[22] Yao X J, Zhang Y, Du L Y, Liu J H and Yao J F 2015 *Renew. Sust. Energ. Rev.* **47** 519

[23] Zhang Z Y and Kong J L 2011 *J. Hazard. Mater.* **193** 325

[24] Socrates G 2001 *Infrared and Raman characteristic group frequencies: tables and charts* (Chichester: Wiley)

[25] Silverstein R M, Webster F X and Kiemle D J 1997 *Spectrometric identification of organic compounds* (New York: Wiley)

[26] Cornell R M and Schwertmann U 2003 *The iron oxides: structure, properties, reactions occurrences and uses* (Wiley: Weinheim)

[27] Bai L, Mei B, Guo Q Z, Shi Z G and Feng Y Q 2010 *J. Chromatogr. A* **121** 77331

[28] Pol V G, Daemen L L, Vogel S and Chertkov G 2010 *Ind. Eng. Chem. Res.* **49** 920

[29] Huang J, Chen W M, Zhao W, Li Y Q, Li X G and Chen C P 2009 *J. Phys. Chem. C* **113** 12067

[30] Tan Y W, Zhuang Z B, Peng Q and Li Y D 2008 *Chem. Mater.* **20** 5029

[31] Zhao W, Yang R J, Qian T T, Hua X, Zhang W B and Katiyo W 2013 *Int. J. Mol. Sci.* **14** 12073

[32] Iram M, Gu C, Guan Y P, Ishfaq A and Liu H Z 2010 *J. Hazard. Mater.* **181** 1039

[33] Konicki W, Cendrowski K, Bazarko G and Mijowska E 2015 *Chem. Eng. Res. Des.* **94** 242

[34] Ahmad R and Kumar R 2010 *J. Environ. Manage.* **91** 1032

[35] Aksu Z and Kabasakal E 2004 *Sep. Purif. Technol.* **35** 223

[36] Ai L H, Huang H Y, Chen Z L, Wei X and Jiang J 2010 *Chem. Eng. J.* **156** 243

[37] Gad H M H and El-Sayed A A 2009 *J. Hazard. Mater.* **168** 1070